IEEE Access
Multidisciplinary | Rapid Review | Open Access Journal

Received October 17, 2020, accepted November 1, 2020, date of publication November 4, 2020, date of current version November 16, 2020.

Digital Object Identifier 10.1109/ACCESS.2020.3035804

A Shape Prior-Based Active Contour Model for Automatic Images Segmentation

XIAOLIANG JIANG[1,2,3] **AND JINYUN JIANG**[1,2]

[1]College of Mechanical Engineering, Quzhou University, Quzhou 324000, China
[2]Key Laboratory of Air-Driven Equipment Technology of Zhejiang Province, Quzhou University, Quzhou 324000, China
[3]College of Mechanical Engineering, Southwest Jiaotong University, Chengdu 610031, China

Corresponding author: Xiaoliang Jiang (jxl_swjtu@163.com)

This work was supported in part by the National Natural Science Foundation of China under Grant 51275272, Grant 51876103, and Grant 51806122, in part by the Zhejiang Provincial Natural Science Foundation of China under Grant LQ17C160001 and Grant LQ18F010007, and in part by the Key Laboratory of Air-driven Equipment Technology of Zhejiang Province under Grant 2018E10011.

ABSTRACT Due to the variable shapes of objects, high noise intensity and complex environments, the field of image segmentation still has great challenges. To address these issues, we present a new image segmentation strategy based on active contour model and shape priori information, which can accurately and efficiently segment various images. The data fitting term, inspired by Chan-Vese (C-V) model, is used to guide the curve evolving to desired target boundary. Meanwhile, the contour is utilized to reconstruct a prior shape so that can help to deal with images in the presence of complex target. After that, the length regularity term of energy functional is incorporated to ensure the stable calculation of the evolution curve. The quantitative and qualitative experiments on various real and medical images indicate that our method is more efficient and accurate than the existing unified models.

INDEX TERMS Image segmentation, active contour, shape prior, level set.

I. INTRODUCTION

Segmentation of medical images can provide doctors with a variety of valuable information, so it plays an important role in many medical applications, such as treatment planning, surgery and prognosis assessment. However, due to the complexity of body anatomy and the diversity of images, it is more difficult to segment medical images than natural images. In traditional medical image diagnosis, the lesions and edges of target are marked manually by radiologists, which is a time-consuming tasks and easily affected by human factors. Therefore, designing an efficient algorithm that can locate, segment, and quantify diseased tissue is of great significance for many clinical treatments.

Considering the characteristics of medical images, many traditional algorithms (such as thresholding, region growing, clustering) cannot meet the requirements of segmentation. As an important branch, active contour model presented by Kass *et al.* [1], also known as snake, has been proved to be efficient approach since the contour can give a closed and stably boundary. Thus, many researchers have done great effort and many methods have been presented to improve it [2]–[5]. Among them, one of the most famous active contour models is the C-V model [6], which utilizes the statistical information to guide the contour. In the C-V model, image intensities in each region are assumed to be statistically homogeneous, thus it cannot provide accurately segment the images with intensity inhomogeneity. To solve the problem of the C-V model, Li *et al.* presented the region scalable fitting (RSF) model [7] based on the local information of the image, which has achieved promising results. However, when an unreasonable initial contour is set, RSF model may fall into local minimum. In [8], Yang *et al.* integrated the local information term and the distance constraint into the variational framework for auroral oval segmentation, thus it can achieve a significantly improvement and obtain more accurate boundaries. Ding *et al.* [9] presented an image segmentation strategy by combining the Laplacian of Gaussian term and the RSF term, which is used to realize an accurate segmentation result. Based on the gravitational search technology, Çataloluk *et al.* [10] implemented an improved C-V model to solve the local minimum problem. Zhang *et al.* [11] presented a modified improved level set algorithm which draws upon the optimized area energy term. With an adaptive edge stopping function, this method can implement a correct segmentation and become more stable. In [5], saliency map

The associate editor coordinating the review of this manuscript and approving it for publication was Naveed Akhtar.

This work is licensed under a Creative Commons Attribution 4.0 License. For more information, see https://creativecommons.org/licenses/by/4.0/

and color intensity are taken into the active contour model as the region external energy to identify a more accurate boundary positioning.

Recently, shape-based active contour models have been constructed to regularize the smoothness of the contour for image segmentation [12]–[16]. Qin *et al.* [17] developed a level set framework for bladder MR image segmentation, which used an adaptive shape priors constrained to obtain the desired boundaries. In another study, based on the intensity information, Pham *et al.* [18] introduced the nonlinear shape priors into the energy functional, which is designed for cardiac MRI images. Yang *et al.* [19] presented an unsupervised prostate segmentation method for hierarchical prostate MRI segmentation. In this approach, the statistics information and shape prior was used in the segmentation task. Research by Meng *et al.* [20] utilized the prior knowledge and the local information term to obtain the outer boundary of the aurora, thus it can provide an accurate segmentation result. Ge et.al [21] improve the imperfection of C-V model based on fuzzy C-means clustering with shape priors, which has better performance and powerful anti-noise capacity. Han et.al [22] used the output of the fully convolutional networks as a probability map, and the improved level set method was employed to segment various images. Finally, both images can obtain accurate segmentation results. Niu et.al [23] created a new active contour model for computed tomography angiography images processing. In the algorithm, shape prior and local region fitting terms are employed. This work achieves the precise segmentation of the epicardial and endocardial parts of the myocardium.

Inspired by the works above-mentioned, we present an adaptive shape prior constrained segmentation algorithm in this paper. The new method can be summarized as follows: Firstly, using the improved C-V model as the data fitting term, we propose a region-based evolution equation. Secondly, the shape prior-based active contour model is built to deal with images in the presence of complex target. Finally, the length regularity term of energy functional is incorporated into the level set framework and the contour is evolved within the narrowed range. The numerical experiments on various real and medical images show that our method is more accurate and efficient than other state-of-the-art methods.

The remainder of the paper is organized as follows: Section 2 briefly introduces the related work. In next Section, the proposed method is discussed. Experiments and results are provided in Section 4, and finally concluding statements are given in Section 5.

II. RELATED WORK

A. C-V MODEL

Chan and Vese presented a simplified Mumford-Shah model [24], which is named C-V model [6]. By assumption that objects of segmenting images have constant brightness, C-V model can accurately segment the images with intensity homogeneity. Let $I : \Omega \rightarrow R^2$ be a given image, C represents the current or initial contour curve. In its most general form, the energy function of C-V is constructed as:

$$\begin{aligned} E^{CV}(C, c_1, c_2) = {} & \nu Area(inside(C)) + \mu Length(C) \\ & + \lambda_1 \int_{inside(C)} |I(x) - c_1|^2 dx \\ & + \lambda_2 \int_{outside(C)} |I(x) - c_2|^2 dx \end{aligned} \tag{1}$$

where λ_1, λ_2, ν, μ are the fitting parameters of each energy items. The values of c_1 and c_2 represent the average intensity values of original image, based on the objects ($inside(C)$) and the background ($outside(C)$).

By replacing C with level set function$\phi(x)$, and introducing the Heaviside function $H_\varepsilon(x)$ and the Dirac function $\delta_\varepsilon(x)$, the Eq. (1) can be modified as:

$$\begin{aligned} E^{CV}(\phi, c_1, c_2) = {} & \nu \int_\Omega H_\varepsilon(\phi) dx + \mu \int_\Omega \delta_\varepsilon(\phi) |\nabla \phi| dx \\ & + \lambda_1 \int_\Omega |I(x) - c_1|^2 H_\varepsilon(\phi) dx \\ & + \lambda_2 \int_\Omega |I(x) - c_2|^2 (1 - H_\varepsilon(\phi)) dx \end{aligned} \tag{2}$$

with

$$H_\varepsilon(x) = \frac{1}{2}\left[1 + \frac{2}{\pi} \arctan\left(\frac{x}{\varepsilon}\right)\right] \tag{3}$$

$$\delta_\varepsilon(x) = H'_\varepsilon(x) = \frac{1}{\pi} \frac{\varepsilon}{\varepsilon^2 + x^2} \tag{4}$$

where ε is a suitably chosen constant.

Subsequently, by applying the gradient descent method, we can get the following equation:

$$\frac{\partial \phi}{\partial t} = \delta_\varepsilon(\phi)[\nu div(\frac{\nabla \phi}{|\nabla \phi|}) - \lambda_1 (I(x) - c_1)^2 + \lambda_2 (I(x) - c_2)^2] \tag{5}$$

with c_1 and c_2 equal to

$$c_1 = \frac{\int_\Omega H_\varepsilon(\phi) I(x) dx}{\int_\Omega H_\varepsilon(\phi) dx}, \quad c_2 = \frac{\int_\Omega (1 - H_\varepsilon(\phi)) I(x) dx}{\int_\Omega (1 - H_\varepsilon(\phi)) dx} \tag{6}$$

Duo to the intensity inside and outside of the curve is assumed to homogeneous, so C-V model will leads to poor segmentation performance with intensity inhomogeneity.

B. LIF MODEL

To segment inhomogeneous images, Zhang *et al.* [25] combined the active contour model with local image fitting (LIF) energy to extract local image information. The energy functional of LIF is expressed as:

$$E^{LIF}(\phi) = \frac{1}{2} \int_\Omega |I(x) - I^{LFI}(x)|^2 dx \tag{7}$$

where $I^{LFI}(x)$ is called a local fitted image, defined by

$$I^{LFI}(x) = H_\varepsilon(\phi) m_1 + (1 - H_\varepsilon(\phi)) m_2 \tag{8}$$

where m_1 and m_2 are formulated as:

$$\begin{cases} m_1 = mean(I \in (\{x \in \Omega | \phi(x) < 0\} \cap W_k(x))) \\ m_2 = mean(I \in (\{x \in \Omega | \phi(x) > 0\} \cap W_k(x))) \end{cases} \tag{9}$$

where $W_k(x)$ is a local window function, with size $(4k+1)\times(4k+1)$ and standard deviation σ. According to the steepest descent method, the energy functional in Eq. (7) can be minimized by:

$$\frac{\partial \phi}{\partial t} = \delta_\varepsilon(\phi)(I - I^{LFI})(m_1 - m_2) \tag{10}$$

Since the LIF model achieves image segmentation by minimizing the difference between the local fitted image and original image, thus, is more efficient and less sensitive to the initial contour. However, this method may produce less accurate when image with heavy noise.

III. PROPOSED METHOD

In this section, we present an active contour model for various real and medical images segmentation. The proposed method consists of three parts: the data fitting term, the shape priori term and the length regularity term. The detailed description is given in detail.

A. DATA FITTING TERM

Inspired by the works of Zhang [25] and Han [26], taking into account the intra-class variances of the pixel inside and outside the contour, a novel active contour model is presented and its objective functional is defined by:

$$E_{data}(\phi) = -\int_\Omega H_\varepsilon(\phi)(c_1 - c_2)(I(x) - (d_1 c_1 + d_2 c_2))dx \tag{11}$$

where d_1 and d_2 the intra-class variances of pixel grayscale values inside and outside the curve contour, which are calculated as:

$$\begin{cases} d_1 = \dfrac{1}{N_1}\displaystyle\int_\Omega H_\varepsilon(\phi)|I(x) - c_1|dx \\ d_2 = \dfrac{1}{N_2}\displaystyle\int_\Omega (1 - H_\varepsilon(\phi))|I(x) - c_1|dx \end{cases} \tag{12}$$

where N_1 and N_2 represent the number of pixels in the corresponding region.

B. SHAPE PRIOR TERM

The data fitting term $E_{data}(\phi)$ proposed in Eq. (11) is sensitive to initial contour, it will result in the wrong segmentation. To solve the above problem, shape constraint information is introduced. Let ϕ be the current evolving shape and ϕ_r is the reference shape, then the shape constraint term can be calculated as:

$$E_{shape}(\phi) = \int_\Omega (H_\varepsilon(\phi) - H_\varepsilon(\phi_r))^2 dx \tag{13}$$

In the process of energy function minimization, when the contour curve of the target deviates from the prior shape constraint, it will be punished. The greater the offset distance is, the greater the penalty is.

C. LEVEL SET FORMULATION

To keep the evolution curve smoothly, the length regularizing term are incorporated into the level set framework, which is defined by:

$$E_{length}(\phi) = \int_\Omega \delta_\varepsilon(\phi)|\nabla\phi|dx \tag{14}$$

Combining the data fitting term, the shape priori term and the length regularity term, then the final energy function of our method is expressed as:

$$E(\phi) = \lambda E_{data}(\phi) + \eta E_{shape}(\phi) + \mu E_{length}(\phi) \tag{15}$$

where λ, η, μ are three parameters.

According to the variational rule and gradient descent method, and the corresponding partial differential equation of Eq. (15) is written as:

$$\begin{aligned}\frac{\partial \phi}{\partial t} &= \lambda\delta_\varepsilon(\phi)(c_1 - c_2)(I(x) - (d_1 c_1 + d_2 c_2)) \\ &\quad - 2\eta\delta_\varepsilon(\phi)(H_\varepsilon(\phi) - H_\varepsilon(\phi_r)) + \mu\delta_\varepsilon(\phi)div(\frac{\nabla\phi}{|\nabla\phi|})\end{aligned} \tag{16}$$

D. IMPLEMENTATION

To improve computational efficiency of the level set method, narrow band technology is used around the closed contour in this paper. Simply, narrow band is defined as:

$$\Omega_{NB} = \{(x, y)|\phi_i^n(x, y)| \le r\} \tag{17}$$

where r is the width of narrow band. In details, we summarize the main procedures of our algorithm as follows:

Step 1: Give an initialized contour inside the object and initialize it to be a binary function $\phi = \phi^0(x)$:

$$\phi^0(x) = \begin{cases} -c_0 & \text{x is inside C} \\ 0 & x \in C \\ c_0 & \text{x is outside C} \end{cases} \tag{18}$$

Step 2: Build the narrow band according to Eq. (17).

Step 3: Compute the points in the narrow band via the evolution Eq. (16).

Step 4: Re-initialize $\phi(x)$ into the binary level set function.

Step 5: Check whether the evolution is stationary. If not, return to step 2.

IV. RESULTS AND ANALYSIS

To verify the processing capability of our method for real and medical images, ACM_LoG [9], ACM_LPF [27], C-V [6], CVXB [28], RSF [7], LRAC [29], Sun's [30], ACLEPF [31], and HLFRA [32] are tested in terms of performance. All experiments are completed by using MATLAB R2014a on the Lenovo desktop (CPU i7-3770 3.4 GHZ and equipped with 4G RAM) running Windows10 operating system (64-bit). Unless otherwise stated, we employ: $\lambda = 1.2$, $\eta = 0.1$, $\mu = 0.2$, $c_0 = 2$, $r = 1.2$.

A. SYNTHETIC IMAGES SEGMENTATION

The first testing experiment is the comparative results of ACM_LoG, ACM_LPF, C-V, CVXB, RSF, LRAC, Sun's, ACLEPF, HLFRA and the proposed model to verify the robustness of the initial contour, where the corresponding

FIGURE 1. Segmentation results of different methods with six initial functions for a plane image. First to last columns are ACM_LoG, ACM_LPF, C-V, CVXB, RSF, LRAC, Sun's, ACLEPF, HLFRA and the proposed model, respectively.

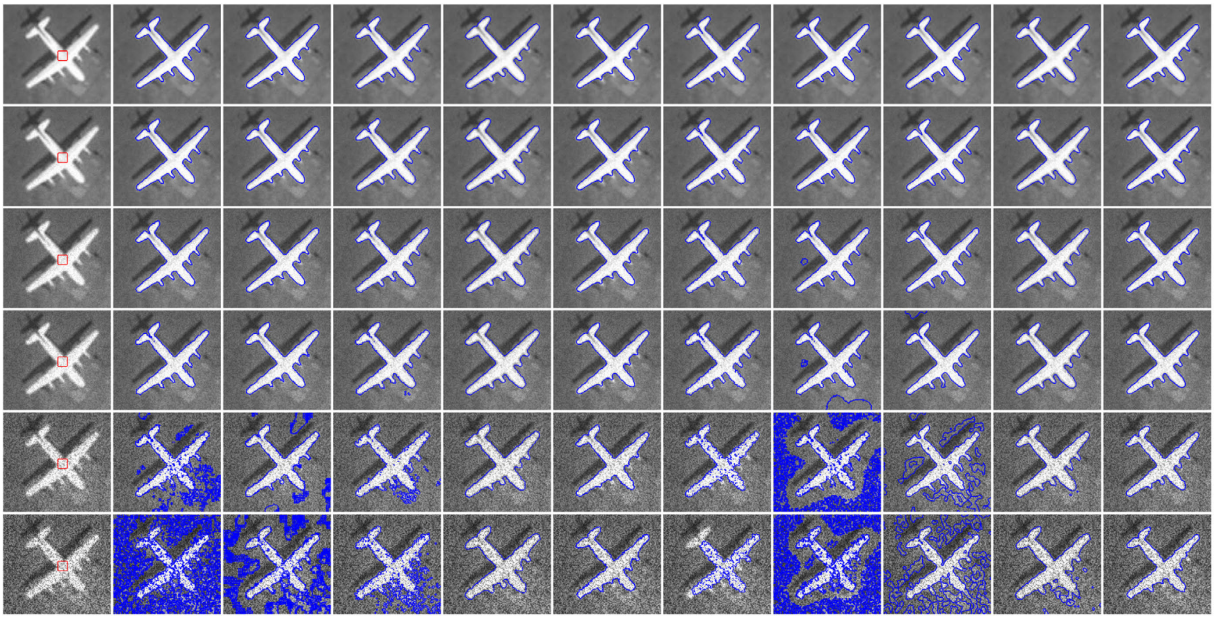

FIGURE 2. Segmentation results for a plane image by different methods with and without speckle noise. First column (up to down): noise-free image, speckle noise images of density 0.001, 0.005, 0.01, 0.05 and 0.1. Second to last columns are results by ACM_LoG, ACM_LPF, C-V, CVXB, RSF, LRAC, Sun's, ACLEPF, HLFRA and the proposed model, respectively.

image is a synthetic plane image (pixel size: 135*125) with distinct shadow, as shown in Fig. 1. According to the experimental results, LRAC, Sun's, and ACLEPF models can segment the image correctly only under some initial contours. However, for the other evaluated methods, each initial contour leads to a desired segmentation result. This shows that the size and location of the initial contour curve has no effect on final results in these models, which establish that our model is robust to the initial contour curve.

As a further comparison, the segmentation results are tested to the above models to show the effectiveness of our method with various noise levels using the plane images. To make a fair experiment, we use the same initializations of the images for all the methods. Firstly, we use speckle noises to evaluate the performance of these different methods. Fig. 2 illustrates the final results with different levels of speckle noises. From up to down, the test images polluted by speckle noise with density levels of 0.001, 0.005, 0.01,

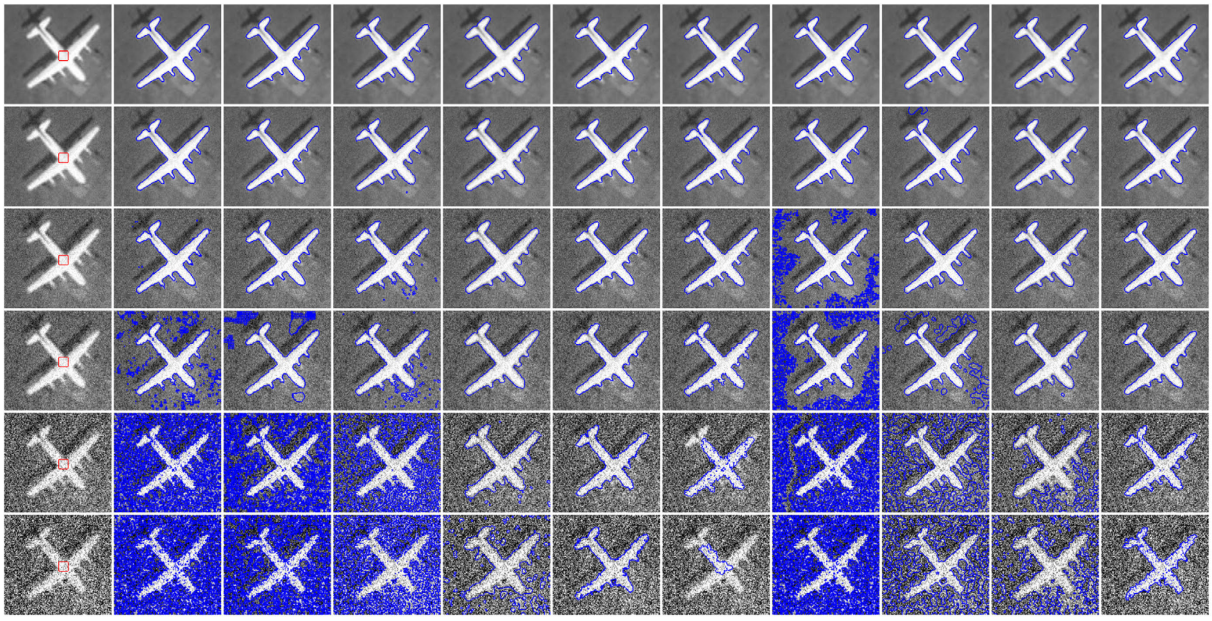

FIGURE 3. Segmentation results for a plane image by different methods with and without Gaussian noise. First column (up to down): noise-free image, Gaussian noise images of density 0.001, 0.005, 0.01, 0.05 and 0.1. Second to last columns are results by ACM_LoG, ACM_LPF, C-V, CVXB, RSF, LRAC, Sun's, ACLEPF, HLFRA and the proposed model, respectively.

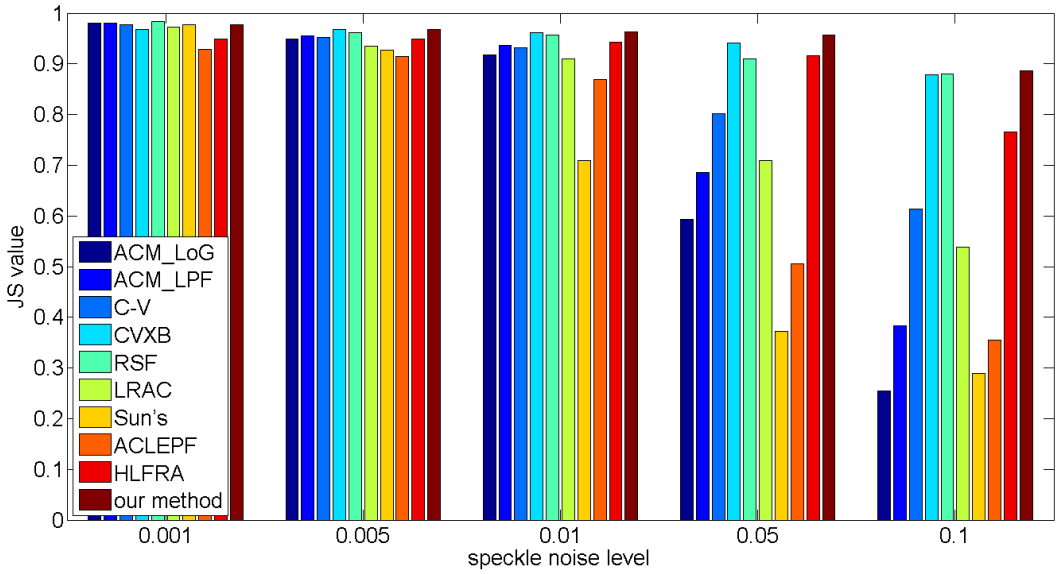

FIGURE 4. Illustration of the JS values for images shown in Fig. 2 with five different levels of speckle noise.

0.05 and 0.1 are shown in the first column, the second to the last columns are the segmentation results obtained by ACM_LoG, ACM_LPF, C-V, CVXB, RSF, LRAC, Sun's, ACLEPF, HLFRA and the proposed model, respectively. We can see that the RSF, LRAC, HLFRA and our method nearly have the best overall performance, which demonstrates that these methods are very robust against speckle noises. For the ACM_LoG, ACM_LPF, C-V, CVXB, Sun's and ACLEPF, when the strength of noises is weak, both of them can get the satisfactory segmentation results. However, when the noise intensity increases, they exhibit poor performance. In order to further validate the robustness of our method, Fig. 3 gives the comparison results of the eight models for images with different levels Gaussian noise (mean 0, variances 0.001, 0.005, 0.01, 0.05, 0.1). In contrast, our model obtained satisfactory segmentation results for the challenging noisy images. For a quantitative comparison, the Jaccard similarity (JS) [33], [34] index is employed to evaluate the images on Figs. 2 and 3. If S_1 and S_2 denote the segmented results obtained by the models and the ground truth respectively, then the metric is defined:

$$JS(S_1, S_2) = \frac{N(S_1 \cap S_2)}{N(S_1 \cup S_2)} \tag{19}$$

where $N(\cdot)$ is the pixels number of the enclosed region. The value of JS ranges from 0 to 1, with a higher value

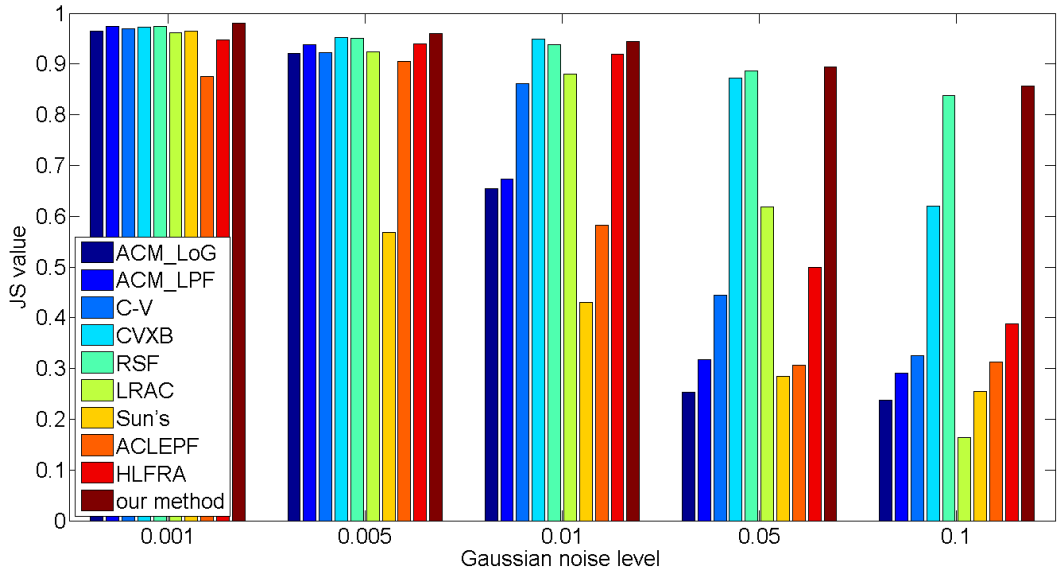

FIGURE 5. Illustration of the JS values for images shown in Fig. 3 with five different levels of Gaussian noise.

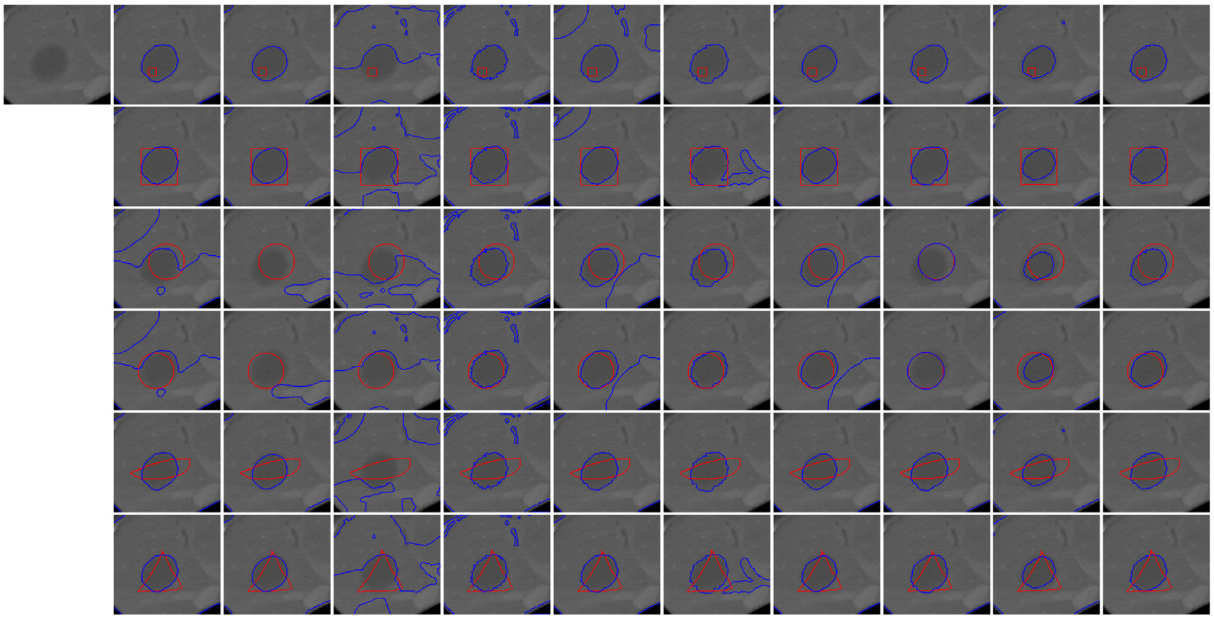

FIGURE 6. Segmentation results of different methods with six initial functions for a computed tomography image. First column: original image. Second to last columns are ACM_LoG, ACM_LPF, C-V, CVXB, RSF, LRAC, Sun's, ACLEPF, HLFRA and the proposed model, respectively. ($\lambda = 0.5$).

representing a better segmentation result. The corresponding JS values are shown in Figs. 4 and 5. From the JS values we can see that, except for individual noise images, the proposed model has the highest JS values among these methods. Therefore, our model could have high and stable segmentation accuracies than other reference methods, qualitatively and quantitatively.

B. MEDICAL IMAGES SEGMENTATION

In the next experiment, these eight models are applied to a computed tomography scans of liver tumor, which has low contrast and weak boundary. As shown in Fig. 6, with different initial contours, C-V cannot segment out the objects, such as the weak boundaries. The ACM_LoG, ACM_LPF, CVXB, RSF, Sun's and ACLEPF are not only sensitive to the initial contours, but also have poor ability to exclude fake objects. Even when the initial contours are set on the correct liver target, it still captures the wrong outline in the background as pseudo object. As shown in the seventh and ninth columns, LRAC and HLFRA are sensitive to initializations and can get promising results to some extent. In contrast, our method is less sensitive to the initial contour and it captures the

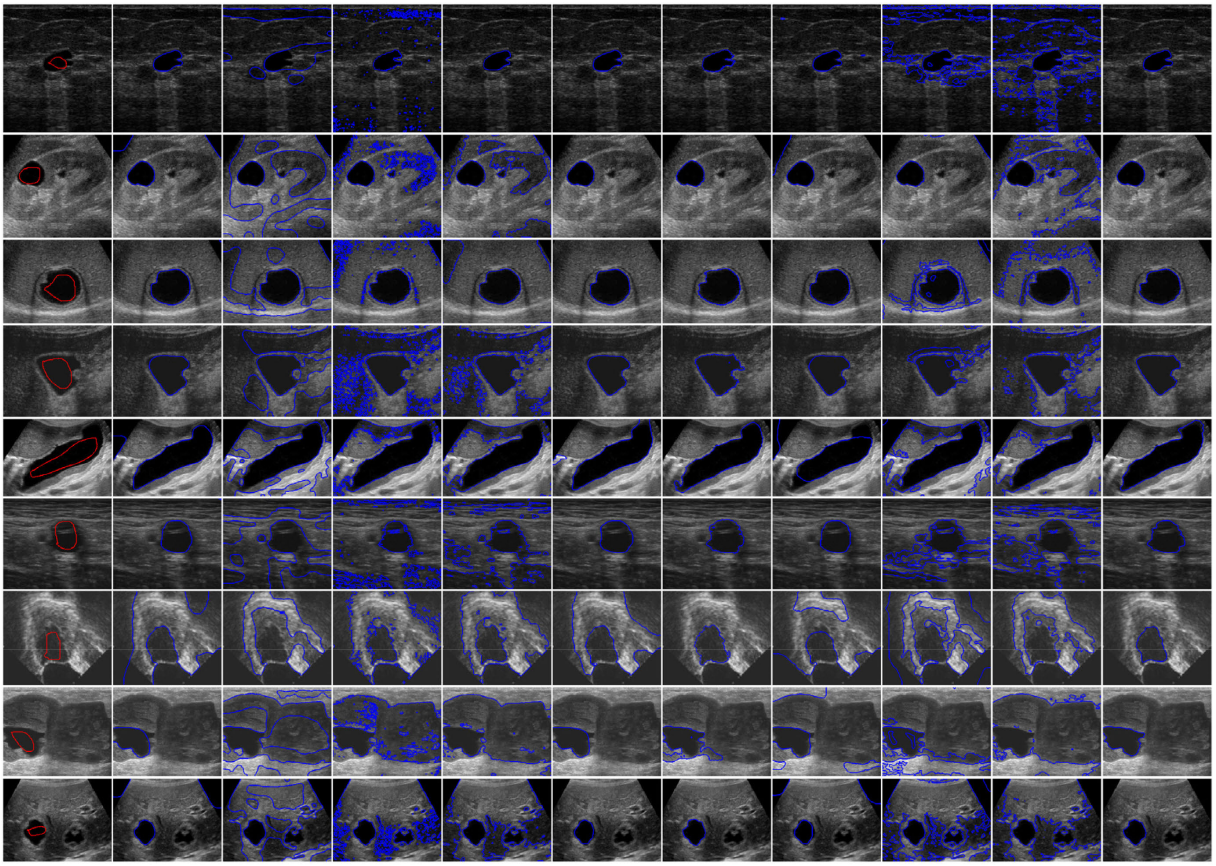

FIGURE 7. Segmentation results of different methods for ultrasound images. First column: original image with red initial contour. Second to last columns are ACM_LoG, ACM_LPF, C-V, CVXB, RSF, LRAC, Sun's, ACLEPF, HLFRA and the proposed model, respectively. ($\lambda = 0.5$).

TABLE 1. Comparison with iterations and computational time (s) for the images in Fig. 7 in the same order

	ACM_LoG		ACM_LPF		C-V		CVXB		RSF		LRAC		Sun's		ACLEPF		HLFRA		Our method	
	Iteration	Time	Iteration	Time	Iteration	Time	Iteration	Time	Iteration	Time	Iteration	Time	Iteration	Time	Iteration	Time	Iteration	Time	Iteration	Time
1	1050	48.13	800	14.88	100	0.10	100	0.29	380	35.63	1100	63.05	400	29.42	100	7.01	40	3.95	200	3.46
2	440	17.26	800	9.70	100	0.09	100	1.62	740	36.76	350	8.97	350	16.94	80	7.17	40	2.96	80	1.08
3	260	9.23	800	7.61	100	0.07	100	0.34	300	11.69	650	12.67	250	9.87	120	5.17	40	2.53	100	1.13
4	280	11.12	800	7.98	100	0.08	100	0.40	340	15.63	600	12.88	350	15.37	80	3.55	40	2.57	160	1.72
5	500	19.41	800	9.43	100	0.08	100	0.57	320	12.04	2000	51.27	700	36.75	100	13.07	40	2.58	300	3.57
6	300	10.62	800	7.88	100	0.07	100	0.66	420	7.86	800	17.68	400	17.72	80	3.72	40	2.49	180	1.88
7	420	11.21	800	4.35	100	0.09	100	0.10	320	13.83	100	1.28	500	9.86	100	3.44	40	1.94	160	0.84
8	500	17.70	800	15.92	100	0.10	100	0.54	320	14.29	1200	29.47	500	26.01	100	4.60	40	2.53	160	1.79
9	900	31.65	800	18.61	100	0.07	100	0.43	900	42.08	300	8.07	600	43.05	80	8.77	40	2.61	120	1.51

liver tumor accurately in all the cases. These illustrate the advantages of our proposed model in processing of medical image and the ability to handle weak boundaries.

In this subsection, experiments on nine representative ultrasound medical images [35], [36] are presented to evaluate the proposed method. The images including intensity inhomogeneities, noise, and blurry boundaries are breast cyst, renal cyst, hydatid cysts with intramural nodules, liquified hematoma, intramural nodule, bronchus, and so on. The contours are manually initialized to irregular areas, as shown the red curve in the first column of Fig. 7. The second to last columns are results of ACM_LoG, ACM_LPF, C-V, CVXB, RSF, LRAC, Sun's, ACLEPF, HLFRA and the proposed model, while the iterations and computational time are list in Table 1. One can get that ACM_LPF, C-V, CVXB, ACLEPF and HLFRA produce severe over-segmentation in most images. The segmentation results of ACM_LoG, RSF, LRAC, and Sun's are subjectively close to the ground truth and most targets can be extracted correctly. Compared with the above models, our method perfectly extracts the desired objects from these images while avoiding boundary leakage and excessive contraction. In addition, from Table 1, we can find that the proposed method arrives at the minimum at a faster speed. This proves that our method is much more feasible.

In order to further verify the superiority of the proposed method, the brain pituitary adenoma images are used in this subsection obtained from Quzhou People's Hospital, Quzhou, China. All images are in the file format of bmp, which are 384*384 pixels in size. In this data set, the ground truths of lesions are constructed by an expert radiologist that listed in the last column of Fig. 8. Similarly, the JS values are used to quantify the outputs of the proposed method and other state-of-art segmentation methods, as shown in Fig. 9. As can

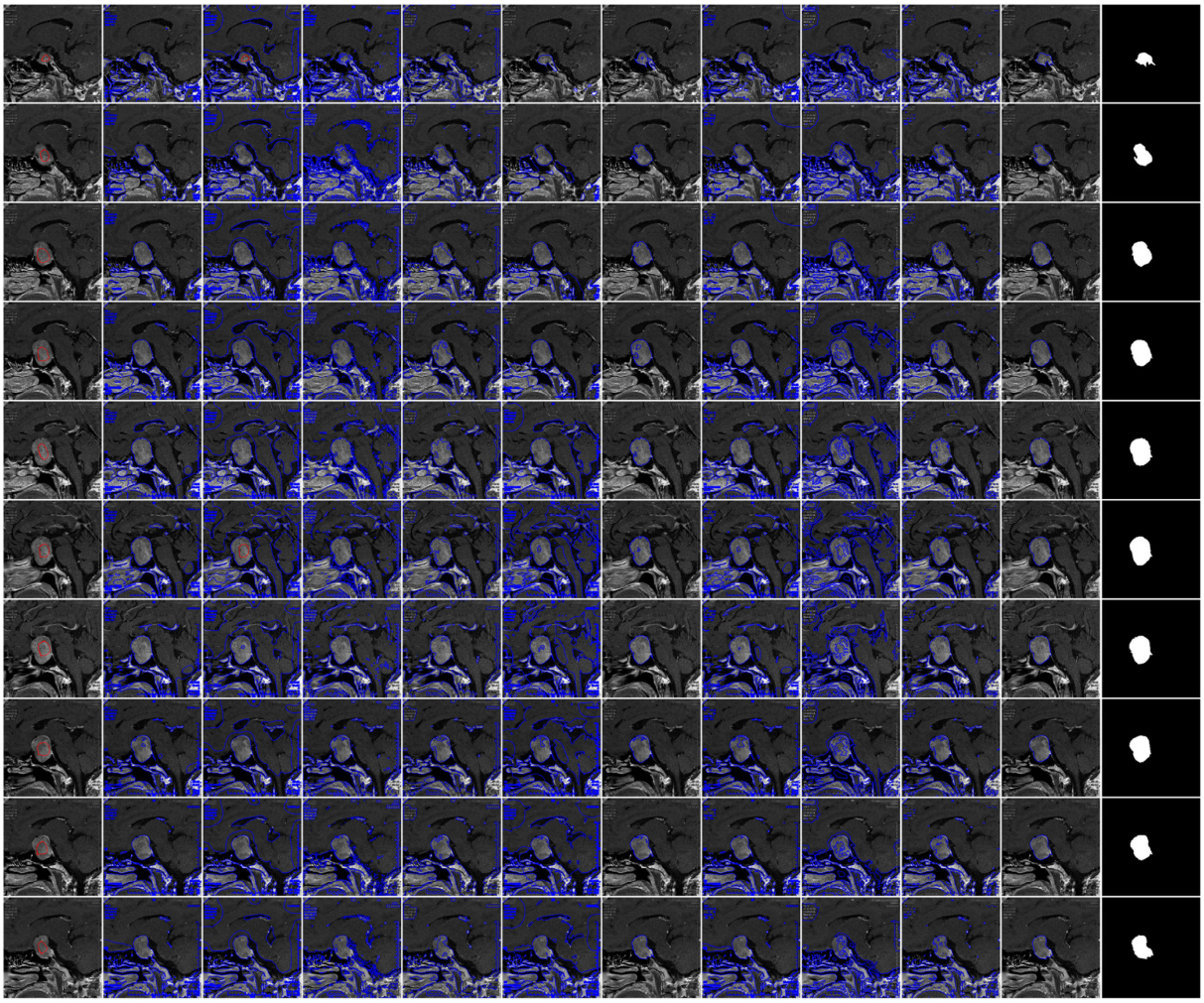

FIGURE 8. Segmentation results of different methods for brain pituitary adenoma images. First column: original image with red initial contour. Second to eleventh columns are ACM_LoG, ACM_LPF, C-V, CVXB, RSF, LRAC, Sun's, ACLEPF, HLFRA and the proposed model. Last column: the ground truth images. ($\lambda = 1.0$).

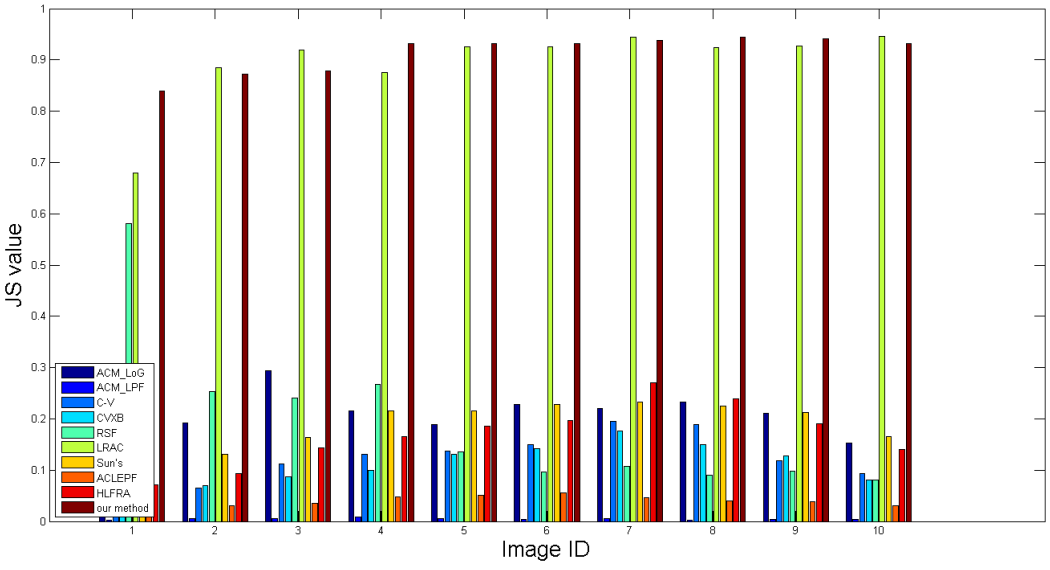

FIGURE 9. Illustration of the JS values for images shown in Fig. 8.

be seen from the experimental results, due to the low contrast, discontinuous boundary and similar surrounding tissues with pituitary adenoma, ACM_LoG, ACM_LPF, C-V, CVXB, RSF, Sun's ACLEPF and HLFRA cannot work properly and

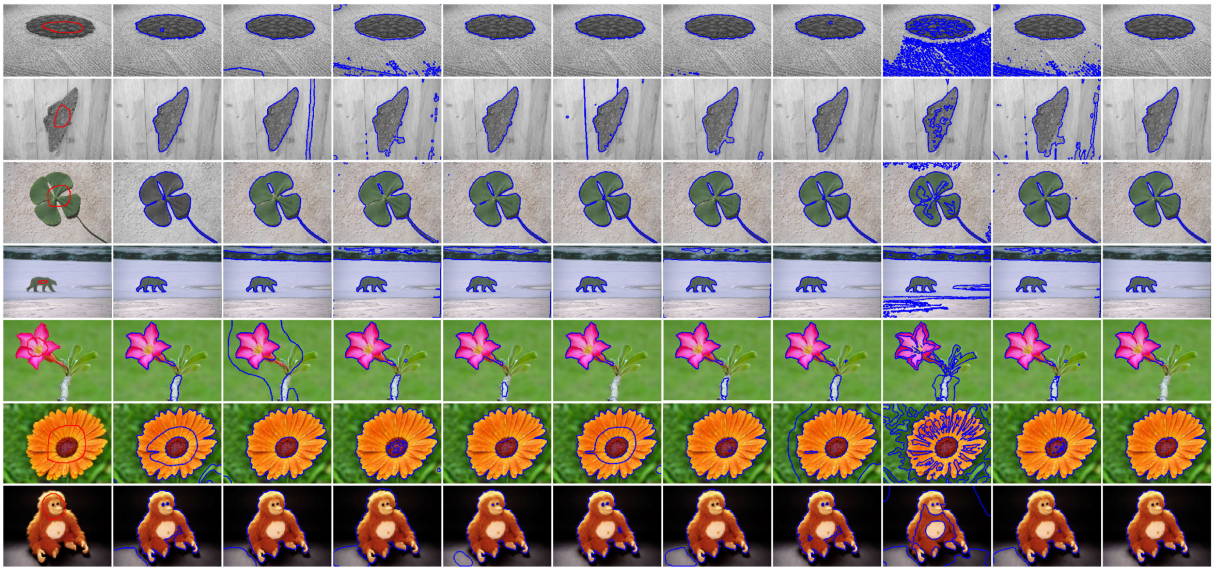

FIGURE 10. Segmentation results of different methods for natural images. First column: original image with red initial contour. Second to last columns are ACM_LoG, ACM_LPF, C-V, CVXB, RSF, LRAC, Sun's, ACLEPF, HLFRA and the proposed model, respectively. (Image 1: $\lambda = 0.6$; Image 2: $\lambda = 0.5$; Image 3: $\lambda = 0.5$; Image 4: $\lambda = 0.6$; Image 5: $\lambda = 0.2$; Image 6: $\lambda = 0.5$; Image 7: $\lambda = 0.7$).

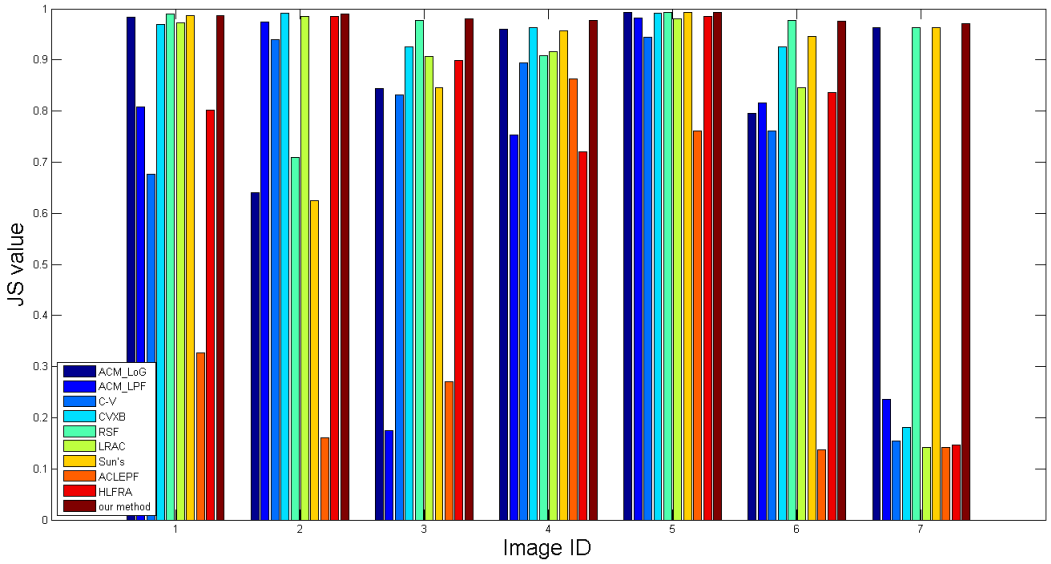

FIGURE 11. Illustration of the JS values for images shown in Fig. 10.

there are a lot of interference in the segmentation results. Nevertheless, LRAC and our method can accurately capture the lesion region, which are close to the ground truth. However, from Fig. 9, we can find that our method is slightly superior to the LRAC model in terms of JS values, and has a great advantage in computing efficiency.

C. NATURAL IMAGES SEGMENTATION

To demonstrate the effectiveness of our method for segmenting complicated nature images, a comparative experiment is tested on seven real images from the MSRA's database and the Berkeley database, and the segmentation results are shown in Fig. 10. It can be seen only the proposed model can exactly extract the objects in every images. The ACM_LPF model is still exists unexpected results to some extent with false detection and gains the worst segmentation effect. Based on the segmentation accuracy, we will employ the JS index to evaluate the performance of each model. From the Fig. 11, it shows that our model is the most stable than these traditional active contour models.

V. CONCLUSION

In this study, we proposed a novel shape prior constrained based approach to for image segmentation. Using the improved C-V model as the data fitting term, the proposed model can guide the curve evolving to desired target boundary quickly. In addition, we introduced the prior shape information to our proposed energy functional. Therefore, the

proposed model can well handle images in the presence of complex target. Experimental results on real and natural images demonstrated that our approach achieves satisfactory results and has more robust against the complex background when compared with other seven representative methods.

REFERENCES

[1] M. Kass, A. Witkin, and D. Terzopoulos, "Snakes: Active contour models," *Int. J. Comput. Vis.*, vol. 1, no. 4, pp. 321–331, Jan. 1988.
[2] S. Pramanik, D. Banik, D. Bhattacharjee, M. Nasipuri, M. K. Bhowmik, and G. Majumdar, "Suspicious-region segmentation from breast thermogram using DLPE-based level set method," *IEEE Trans. Med. Imag.*, vol. 38, no. 2, pp. 572–584, Feb. 2019.
[3] C. Ma, G. Luo, and K. Wang, "Concatenated and connected random forests with multiscale patch driven active contour model for automated brain tumor segmentation of MR images," *IEEE Trans. Med. Imag.*, vol. 37, no. 8, pp. 1943–1954, Aug. 2018.
[4] C. Liu, W. Liu, and W. Xing, "A weighted edge-based level set method based on multi-local statistical information for noisy image segmentation," *J. Vis. Commun. Image Represent.*, vol. 59, pp. 89–107, Feb. 2019.
[5] X.-H. Zhi and H.-B. Shen, "Saliency driven region-edge-based top down level set evolution reveals the asynchronous focus in image segmentation," *Pattern Recognit.*, vol. 80, pp. 241–255, Aug. 2018.
[6] T. F. Chan and L. A. Vese, "Active contours without edges," *IEEE Trans. Image Process.*, vol. 10, no. 2, pp. 266–277, Feb. 2001.
[7] C. Li, C.-Y. Kao, J. C. Gore, and Z. Ding, "Minimization of region-scalable fitting energy for image segmentation," *IEEE Trans. Image Process.*, vol. 17, no. 10, pp. 1940–1949, Oct. 2008.
[8] P. Yang, Z. Zhou, H. Shi, and Y. Meng, "Auroral oval segmentation using dual level set based on local information," *Remote Sens. Lett.*, vol. 8, no. 12, pp. 1112–1121, Dec. 2017.
[9] K. Ding, L. Xiao, and G. Weng, "Active contours driven by region-scalable fitting and optimized Laplacian of Gaussian energy for image segmentation," *Signal Process.*, vol. 134, pp. 224–233, May 2017.
[10] H. Çataloluk and F. V. Çelebi, "A novel hybrid model for two-phase image segmentation: GSA based Chan-Vese algorithm," *Eng. Appl. Artif. Intell.*, vol. 73, pp. 22–30, 2018.
[11] X. Zhang and G. Weng, "Level set evolution driven by optimized area energy term for image segmentation," *Optik*, vol. 168, pp. 517–532, Sep. 2018.
[12] N. Martins, S. Sultan, D. Veiga, M. Ferreira, F. Teixeira, and M. Coimbra, "A new active contours approach for finger extensor tendon segmentation in ultrasound images using prior knowledge and phase symmetry," *IEEE J. Biomed. Health Informat.*, vol. 22, no. 4, pp. 1261–1268, Jul. 2018.
[13] H. Sui, K. An, C. Xu, J. Liu, and W. Feng, "Flood detection in PolSAR images based on level set method considering prior geoinformation," *IEEE Geosci. Remote Sens. Lett.*, vol. 15, no. 5, pp. 699–703, May 2018.
[14] S. Yan, X.-C. Tai, J. Liu, and H.-Y. Huang, "Convexity shape prior for level set-based image segmentation method," *IEEE Trans. Image Process.*, vol. 29, pp. 7141–7152, 2020.
[15] A. Eltanboly, M. Ghazal, H. Hajjdiab, A. Shalaby, A. Switala, A. Mahmoud, P. Sahoo, M. El-Azab, and A. El-Baz, "Level sets-based image segmentation approach using statistical shape priors," *Appl. Math. Comput.*, vol. 340, pp. 164–179, Jan. 2019.
[16] Z. Zhou, M. Dai, T. Wang, and R. Zhao, "Prior distribution-based statistical active contour model," *Multimedia Tools Appl.*, vol. 78, no. 24, pp. 35813–35833, Dec. 2019.
[17] X. Qin, X. Li, Y. Liu, H. Lu, and P. Yan, "Adaptive shape prior constrained level sets for bladder MR image segmentation," *IEEE J. Biomed. Health Informat.*, vol. 18, no. 5, pp. 1707–1716, Sep. 2014.
[18] V.-T. Pham and T.-T. Tran, "Active contour model and nonlinear shape priors with application to left ventricle segmentation in cardiac MR images," *Optik*, vol. 127, no. 3, pp. 991–1002, Feb. 2016.
[19] X. Yang, S. Zhan, D. Xie, H. Zhao, and T. Kurihara, "Hierarchical prostate MRI segmentation via level set clustering with shape prior," *Neurocomputing*, vol. 257, pp. 154–163, Sep. 2017.
[20] Y. Meng, Z. Zhou, Y. Liu, Q. Luo, P. Yang, and M. Li, "A prior shape-based level-set method for auroral oval segmentation," *Remote Sens. Lett.*, vol. 10, no. 3, pp. 292–301, Mar. 2019.
[21] S. Ge, Z. Shi, G. Peng, and Z. Zhu, "Two-steps coronary artery segmentation algorithm based on improved level set model in combination with weighted shape-prior constraints," *J. Med. Syst.*, vol. 43, no. 7, p. 210, Jul. 2019.
[22] Y. Han, S. Zhang, Z. Geng, Q. Wei, and Z. Ouyang, "Level set based shape prior and deep learning for image segmentation," *IET Image Process.*, vol. 14, no. 1, pp. 183–191, Jan. 2020.
[23] Y. Niu, L. Qin, and X. Wang, "Structured graph regularized shape prior and cross-entropy induced active contour model for myocardium segmentation in CTA images," *Neurocomputing*, vol. 357, pp. 215–230, Sep. 2019.
[24] D. Mumford and J. Shah, "Optimal approximations by piecewise smooth functions and associated variational problems," *Commun. Pure Appl. Math.*, vol. 42, no. 5, pp. 577–685, Jul. 1989.
[25] K. H. Zhang, H. Song, and L. Zhang, "Active contours driven by local image fitting energy," *Pattern Recognit.*, vol. 43, no. 4, pp. 1199–1206, 2010.
[26] B. Han, Y. Wu, and A. Basu, "An adaptive active contour model driven by weighted local and global image fitting constraints for image segmentation," *Signal, Image Video Process.*, vol. 14, no. 1, pp. 1–8, Feb. 2020.
[27] K. Ding, L. Xiao, and G. Weng, "Active contours driven by local pre-fitting energy for fast image segmentation," *Pattern Recognit. Lett.*, vol. 104, pp. 29–36, Mar. 2018.
[28] D. Zosso, J. An, J. Stevick, N. Takaki, M. Weiss, L. S. Slaughter, H. H. Cao, P. S. Weiss, and A. L. Bertozzi, "Image segmentation with dynamic artifacts detection and bias correction," *Inverse Probl. Imag.*, vol. 11, no. 3, pp. 577–600, 2017.
[29] S. Lankton and A. Tannenbaum, "Localizing region-based active contours," *IEEE Trans. Image Process.*, vol. 17, no. 11, pp. 2029–2039, Nov. 2008.
[30] K. Sun, Y. Li, S. Zeng, and J. Wang, "Hybrid active contour model for inhomogeneous image segmentation with background estimation," *J. Electron. Imag.*, vol. 27, no. 2, 2018, Art. no. 023018.
[31] H. Liu, J. Fang, Z. Zhang, and Y. Lin, "A novel active contour model guided by global and local signed energy-based pressure force," *IEEE Access*, vol. 8, pp. 59412–59426, 2020.
[32] J. Fang, H. Liu, L. Zhang, J. Liu, and H. Liu, "Region-edge-based active contours driven by hybrid and local fuzzy region-based energy for image segmentation," *Inf. Sci.*, vol. 546, pp. 397–419, Feb. 2021.
[33] K. Zhang, L. Zhang, H. Song, and W. Zhou, "Active contours with selective local or global segmentation: A new formulation and level set method," *Image Vis. Comput.*, vol. 28, no. 4, pp. 668–676, Apr. 2010.
[34] H.-H. Chang, A. H. Zhuang, D. J. Valentino, and W.-C. Chu, "Performance measure characterization for evaluating NeuroImage segmentation algorithms," *NeuroImage*, vol. 47, no. 1, pp. 122–135, Aug. 2009.
[35] L. Fang, T. Qiu, Y. Liu, and C. Chen, "Active contour model driven by global and local intensity information for ultrasound image segmentation," *Comput. Math. Appl.*, vol. 75, no. 12, pp. 4286–4299, Jun. 2018.
[36] J.-J. Zong, T.-S. Qiu, W.-D. Li, and D.-M. Guo, "Automatic ultrasound image segmentation based on local entropy and active contour model," *Comput. Math. Appl.*, vol. 78, no. 3, pp. 929–943, Aug. 2019.

XIAOLIANG JIANG received the M.S. and Ph.D. degrees in mechanical design from Southwest Jiaotong University, Chengdu, China, where he is currently an Associate Professor with Quzhou University. His research interests include machine vision and image recognition.

JINYUN JIANG received the M.S. degree in mechanical design and theory from the Beijing University of Chemical Technology, Beijing, China. Her research interests include material processing and image segmentation.